Activated twinning variant determination in cold-rolled 316L stainless steel by effective Schmid factor analysis

Louis Lemarquis, Pierre-Francois Giroux, Hicham Maskrot, Philippe Castany

Activated twinning variant determination in cold-rolled 316L stainless steel by effective Schmid factor analysis

Louis Lemarquis[a,b], Pierre-François Giroux[a], Hicham Maskrot[a], Philippe Castany[b,*]

[a] *Université Paris-Saclay, CEA, Service de Recherche en Matériaux et procédés Avancés, Gif-sur-Yvette, F-91191, France*
[b] *Univ Rennes, INSA Rennes, CNRS, ISCR - UMR 6226, Rennes, F-35000, France*

Abstract

A method is proposed to determine accurately the activated twinning variant during the cold-rolling of 316L stainless steel parts produced by L-PBF (Laser Powder Bed Fusion) from EBSD datas. The twinning variant selection is carried out by Schmid factor (SF) computations, using an effective Schmid factor for cold-rolling specifically. Schmid factor was proven to be a relevant parameter to predict the experimentally activated twinning variant. Additionally, cold-rolling deformation is shown to be composed by a strong compression component, along with a minor traction component. The effective Schmid factor is then modified accordingly to ensure a better prediction of twinned grains. Moreover, twinning Schmid factor analyses in traction and compression provide valuable information on the twinning activation regarding textured materials such as L-PBF 316L steel.

Keywords: 316L Stainless steel, Cold-Rolling, Additive Manufacturing, Twinning, Schmid factor

*Corresponding author : philippe.castany@insa-rennes.fr

PACS: 0000, 1111
2000 MSC: 0000, 1111

Stainless steels, such as 304L or 316L grades, have a wide range of usage, from biomedical to nuclear applications [1, 2]. 316L stainless steel is a face-centered cubic (fcc) structure material and can be subject to several deformation mechanisms: dislocation slip, deformation twinning or strain-induced martensitic transformation when reaching high levels of deformation [3, 4]. Regarding twinning, $\{111\}\langle 1\,1\,2\rangle$ is the usual twinning system of fcc metals and alloys with 12 ways to be activated, named variants. The signs of indices of twinning plane and direction have to be determined carefully to allow SF calculation for twinning [5] and are shown in Table 1 for fcc structures.

The Schmid law is frequently used to predict the activated slip system depending on the local tensile or compression directions compared with the crystallographic orientation of the considered grain. However, several studies used also the Schmid law to predict twinning variants in bcc or fcc structures [5, 6]. While Schmid factor analysis is common for uniaxial loading, Luo et al. [7] proposed a modified Schmid factor component in order to analyse the twinning behaviour of a AZ31 Mg alloy during warm-rolling. This modified Schmid factor takes into consideration both Schmid factors for tension along the rolling direction and compression along the sheet normal direction in an effective Schmid factor suitable for rolling. The main goal of this paper is to propose a robust protocol to identify the activated twinning variants and rationalise their activation during cold-rolling by a Schmid factor analysis. As a material of investigation, additively manufactured 316L steel is used

after subsequent cold-rolling. The influence of the tension and compression components in the twinning variant activation during rolling is particularly highlighted.

Variant	$\{1\ 1\ 1\}$ Plane	$\langle 1\,1\,2\rangle$ Direction
01	$(1\ 1\ 1)$	$[1\ 1\ \overline{2}]$
02	$(1\ 1\ 1)$	$[\overline{2}\ 1\ 1]$
03	$(1\ 1\ 1)$	$[1\ \overline{2}\ 1]$
04	$(1\ \overline{1}\ 1)$	$[1\ 2\ 1]$
05	$(1\ \overline{1}\ 1)$	$[1\ \overline{1}\ \overline{2}]$
06	$(1\ \overline{1}\ 1)$	$[\overline{2}\ \overline{1}\ 1]$
07	$(\overline{1}\ 1\ 1)$	$[2\ 1\ 1]$
08	$(\overline{1}\ 1\ 1)$	$[\overline{1}\ \overline{2}\ 1]$
09	$(\overline{1}\ 1\ 1)$	$[\overline{1}\ 1\ \overline{2}]$
10	$(1\ 1\ \overline{1})$	$[1\ 1\ 2]$
11	$(1\ 1\ \overline{1})$	$[\overline{2}\ 1\ \overline{1}]$
12	$(1\ 1\ \overline{1})$	$[1\ \overline{2}\ \overline{1}]$

Table 1: The 12 variants of the $\{111\}\langle 1\,1\,2\rangle$ twinning systems of fcc structures.

316L stainless steel preforms with dimensions of 60*20*15 mm^3 were fabricated using a commercial L-PBF (Laser Powder Bed Fusion) machine ($SLM280^{HL}$, SLM Solutions GmbH, Germany) and 316L steel powder provided by SLM Solutions. The building direction lies along the longest direction of the preforms. Powder characteristics were summarised in details in a previous study [8]. During the construction process, laser power, scan speed,

hatch distance and layer thickness were set at 175W, 750mm/s, 100µm and 30µm, respectively. The scan strategy, developed by SLM Solutions, consists of a raster scanning strategy with 7mm-wide strips and a rotation angle of 67° between layers [8]. A relative density of 99.7% (Archimede) was reached using these process parameters. The as-built preforms were buffed and sanded to remove the building supports and for surface finishing. The preforms were then cold-rolled up to 10% thickness reduction using a unidirectional rolling mill. The rolling direction is collinear to the building direction.

Microstructural analyses were performed by using scanning electron microscopy (SEM; Jeol-7000F) with an electron backscattered diffraction detector (EBSD, Bruker) at different magnifications. Data acquisition was made with an accelerating voltage of 15 kV, a current density of 10 nA, a working distance of 16 mm and a step size of 0.09 µm. The samples were final-polished using a colloidal 1µm-diamond solution to achieve a mirror surface finishing. Successive electrolytic polishing and etching were then performed using a 10 wt% oxalic acid solution at 15V and 10V respectively. EBSD post-processing was carried out by the ESPRIT software from Bruker in order to get the Euler angles of each grain. Stereographic projection calculations were constructed using the CaRIne Crystallography software.

Several twinned microstructures and grains were characterised by EBSD measurements and a meaningful example of an EBSD map is given in Figure 1. Grains of interest (labelled A, B, C and D) are selected to highlight typical observed cases. In this paper, BD = Building Direction; RD = Rolling Direction; ND = Normal Direction; TD = Transverse Direction.

For each analysed grain, crystallographic orientations of the parent crystal

and twins are first determined from their Euler angles. As an illustration, the protocol is exposed by analysing the microstructure shown in Figure 1. The stereographic projection of the parent crystal is first reconstructed thanks to the Euler angles obtained from the EBSD data. The crystallographic directions for RD and ND, respectively the tensile and compression axes during cold-rolling, are identified as shown in Figure 2a for the grain labeled A in Figure 1. The equality of both strain and stress tensors between the grain-scale and the macroscopic scale of the preform ensures the correspondence of tensile and compression axes of each grain with the macroscopic tensile and compression axes, respectively. This equality is a strong condition that cannot be fulfilled for high deformation levels, that is why the present study only considers 10% cold-rolled samples, i.e. the early stage of deformation.

From the RD and ND directions, Schmid factor (SF) are computed for each twin variant: a Schmid factor related to an uniaxial tensile stress along RD (SF_{RD}), a Schmid factor related to an uniaxial compressive stress perpendicular to RD and along ND (SF_{ND}) and an effective Schmid factor for rolling as proposed by Luo et al. [7] taking these two previous components into account (SF_{Eff}):

$$SF_{Eff} = \frac{1}{2}[\cos(\varphi_{RD})\cos(\lambda_{RD}) - \cos(\varphi_{ND})\cos(\lambda_{ND})] = \frac{1}{2}[SF_{RD} - SF_{ND}] \tag{1}$$

where φ_{RD} and λ_{RD} are respectively the angles between the twin plane normal, and the twin direction, with the rolling direction RD. φ_{ND} and λ_{ND} are respectively the angles between the twin plane normal, and the twin direction, with the normal direction ND. It is also noticed that the signs of

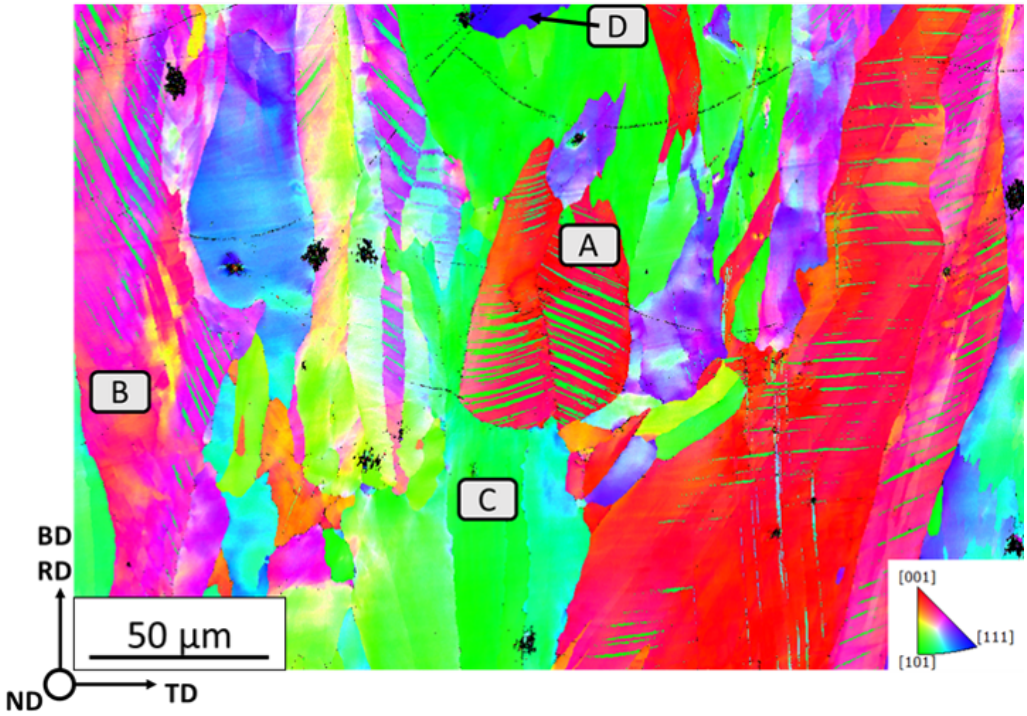

Figure 1: EBSD Inverse Pole Figure (IPF) map from the transverse cross section (RD,TD) of L-PBF 316L after 10% cold-rolling along BD. The orientations shown by the IPF map are related to the normal direction (||ND).

crystallographic indices of twinning plane and direction must be carefully chosen for accurate SF calculations for twinning [5]. From this definition, negative values of SF indicate a contraction of the crystal along the stress direction and, in turn, compression twinning variants. The opposite occurs for positive values of SF, indicating an elongation of the crystal and then tensile twinning variants. Thus, values of SF_{RD}, SF_{ND} and SF_{Eff} can be computed for each variant of the considered grain A of Figure 1 as shown in Table 2. The variant with the highest absolute value of Schmid factor is

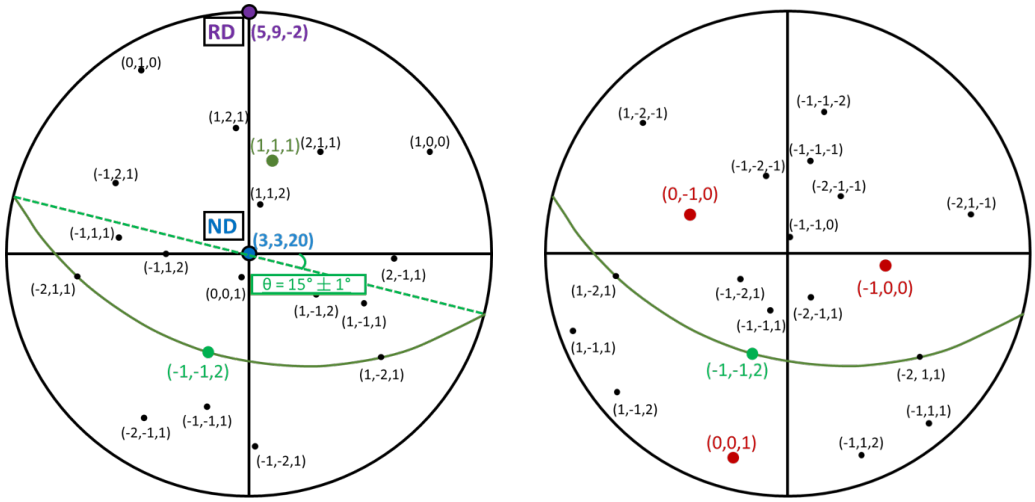

(a) (b)

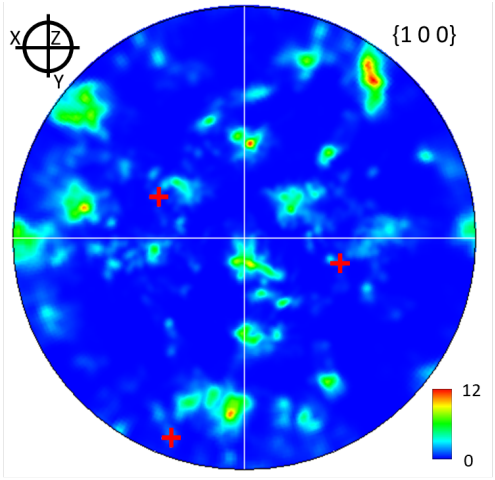

(c)

Figure 2: Stereographic projection of grain A (a) and twins inside (b) with {111} and {112} poles. RD and ND directions are shown, as well as the pole of the activated twinning plane and its corresponding trace in green. Experimental {1 0 0} pole figure from the EBSD analysis (c); Red markers are {1 0 0} poles of the twin.

then the most likely to be experimentally activated. Then, positive values of SF_{RD} close to 0.5 indicate favorable variants regarding a tension along RD, negative values of SF_{ND} close to -0.5 indicate favorable variants regarding a compression along ND and positive values of SF_{Eff} close to 0.5 indicate favorable variants by considering an effective SF for rolling. In the presented case, Schmid factors are very favorable for the twin variant A01 as all the considered SF values are over 0.45 in absolute terms.

Variant	SF_{RD}	SF_{ND}	SF_{Eff}
A01	**0.46**	**-0.50**	**0.48**
A02	-0.08	0.25	-0.16
A03	-0.39	0.25	-0.32
A04	-0.27	0.33	-0.30
A05	0.00	-0.45	0.23
A06	0.27	0.12	0.07
A07	0.07	0.33	-0.13
A08	-0.11	0.12	-0.12
A09	0.03	-0.45	0.24
A10	0.34	-0.36	0.35
A11	0.03	0.18	-0.07
A12	-0.38	0.18	-0.28

Table 2: Values of SF_{RD}, SF_{ND} and SF_{Eff} for the 12 variants of grain A.

Two parameters were then used to check that this particular variant A01 was actually activated after 10% cold-rolling. First, the angle θ formed by the

expected twinning plane, shown in green on Figure 2a, should be the same than the angle exhibited by the twinning plane on the EBSD map of Figure 1. Secondly, the crystallographic orientation of the twinned crystal (Figure 2b) computed by applying the twinning relationship to the stereographic projection of the parent crystal has to be the same than the actual crystallographic orientation of the twin obtained from EBSD data (Figure 2c). These two points allow to determine unambiguously the twinning plane, for which three twinning variants remain, each one corresponding to a different $\langle 1\,1\,2 \rangle$ twinning direction. As these three variants cannot be distinguished, the activated variant is chosen to be the one with the highest Schmid factor values, as one of these is systematically much higher than the two others.

For this particular example, the trace of the (1 1 1) plane (Figure 2a) and the grain-twin interface in the EBSD map (Figure 1) are very close, with angle values of 15°±2° and 20°±5°, respectively, while the angles for the other {1 1 1} planes are all higher than 40°. For this (1 1 1) twinning plane, three twinning directions are possible corresponding to 01, 02 and 03 variants (Table 1). As SF values (Table 2) are obviously unfavorable for the variants A02 and A03, the variant A01 can reliably be considered as the activated one.

This protocol allows to accurately determine the activated twin variant and is used for all twins observed in grains B, C and D on Figure 1. For these grains, the variants possessing $\mathrm{SF}_{RD} \geq 0.35$, or $\mathrm{SF}_{ND} \leq$ -0.35, or $\mathrm{SF}_{Eff} \geq$ 0.25 are given in Table 3.

From the EBSD analysis presented in Figure 1, grains A and B show mechanical twinning, whereas grains C and D do not. In grain A, the experi-

mentally observed variant (A01) has the highest SF value among the variants of the $\{1\ 1\ 1\}\langle 1\,1\,2\rangle$ system (Table 2). In grain B, the activated variant B10 is exhibiting SF_{RD}=0.17, SF_{ND}=-0.41 and SF_{Eff}=0.29 (Table 3). However, variant B05 shows more favorable SF values with slightly higher SF_{Eff} (0.34) and SF_{RD} (0.32) values, but a slightly lower value of SF_{ND} (-0.37). SF_{ND} value is also lower in absolute terms for variants B02, B05 and B09, compared to variant B10. Therefore, the activated twinning variant is not necessarily the one having the highest SF_{Eff} value. This grain shows that SF_{Eff} cannot accurately predict the activated twin variant and that SF_{ND} seems to have a more important effect than SF_{RD}, as a very low of SF_{RD} combined with a high value of SF_{ND} allows the twin variant to be activated. This point will be discussed in the following.

Variant	SF_{RD}	SF_{ND}	SF_{Eff}
B02	0.39	0.07	0.16
B05	0.32	-0.37	0.34
B09	0.17	-0.37	0.27
B10	**0.17**	**-0.41**	**0.29**
C02	0.46	0.00	0.23
C07	0.48	0.00	0.24
D02	0.50	-0.14	0.32
D07	0.37	-0.23	0.30

Table 3: Values of SF_{RD}, SF_{ND} and SF_{Eff} for the 12 variants of grain B, C and D.

Grain C does not exhibit mechanical twins while having two twinning

variants with very favorable SF_{RD} values, 0.46 and 0.48. However, SF_{ND} are equal to 0 for both considered variants. Consequently, and conversely to grain B, a twin variant is not activated with a combination of a very high value of SF_{RD} and a very low value of SF_{ND}. This grain demonstrates again that the compression along ND has a greater effect than the tensile component along RD. Grain D does not exhibit mechanical twinning either, while having two twinning variants with higher SF values than grain C (Table 3): for example, variant D02 gets SF_{RD}=0.50, SF_{ND}=-0.14 and SF_{Eff}=0.32. Compared to the variant B10 of grain B that was activated with a slightly lower SF_{Eff} value of 0.29, the main difference is the inversion of SF_{RD} and SF_{ND} values. The compression component is then strongly preponderant in comparison with the tensile component in the activation of twin variants, that makes the use of SF_{Eff} not fully satisfactory in the present state.

Therefore, in order to predict more accurately the activated twin variant during cold-rolling of 316L L-PBF parts, a modification of the definition of SF_{Eff} given in Equation 1 is proposed to give more weight to the compressive component by adding two factors A and B (with $B \gg A$):

$$SF_{Eff-rolling} = \frac{1}{2}[A\cos(\varphi_{RD})\cos(\lambda_{RD}) - B\cos(\varphi_{ND})\cos(\lambda_{ND})] \quad (2)$$

From the present results, the values of the coefficients can be empirically estimated to ensure that activated twin variants have the highest $SF_{Eff-rolling}$ value : $A = 0.15$ and $B = 1.85$. Thus, an $SF_{Eff-rolling}$ value ranging between 0.35 and 0.50 indicates that the corresponding variant will be activated in the considered grain without considering SF_{RD} and SF_{ND} separately (Table 4). Furthermore, in the case of grain B, the modified $SF_{Eff-rolling}$ leads to a more

coherent hierarchy between all variants with the activated one being the one with the highest value (B10). The validity of this modification was confirmed statistically by a broader analysis on numerous grains in several cold-rolled specimens. Thus, an empirical criterion to predict the activation of twinning in a specific grain during cold-rolling can be established as $SF_{Eff-rolling} \geq 0.38$. If such condition is observed, all analysed grains are shown to be twinned. However, for grains with $0.30 < SF_{Eff-rolling} < 0.38$, some are twinned and some not, that could be explained by a stronger competition between twinning and dislocation slip, these grains being most probably more favorably orientated for dislocation slip.

Variant	SF_{RD}	SF_{ND}	$SF_{Eff-rolling}$
B02	0.39	0.07	0.09
B05	0.32	-0.37	0.36
B09	0.17	-0.37	0.35
B10	**0.17**	**-0.41**	**0.39**
C02	0.46	0.00	0.03
C07	0.48	0.00	0.04
D02	0.50	-0.14	0.24
D07	0.37	-0.23	0.21

Table 4: Values of SF_{RD}, SF_{ND} and $SF_{Eff-rolling}$ for the 12 variants of grains B, C and D.

Therefore, the use of SF to predict the activated twin variant during cold-rolling is valid after 10% reduction rate, but not necessarily for higher

deformation. Indeed, at higher cold-rolling rate, the local stress direction can deviate from the macroscopic one and, in turn, makes SF calculations inaccurate. This feature was observed in specimens after 20% cold-rolling, for which some grains with $\mathrm{SF}_{Eff-rolling}$ values below 0.2 exhibit mechanical twins. Nevertheless, all grains with $\mathrm{SF}_{Eff-rolling}$ values close to 0.5 show twinning activation. The previous criterion $\mathrm{SF}_{Eff-rolling} \geq 0.38$ is then only reliable to predict twinning activation in the early stages of deformation. It has also to be pointed out that additively manufactured steels exhibit a dislocation cell structure that facilitates twinning nucleation [9]. Twinning is then expected to be activated at lower cold-rolling rate in additively manufactured materials in comparison with steels produced from conventional routes, regardless of any potential effects from crystallographic orientation. Thus, the previous analysis should be suitable for any production route and any fcc material.

While SF_{RD} and SF_{ND} (only considering uniaxial stresses) are not suitable to predict twinning activation during cold-rolling, they can be used to determine the favorable crystallographic orientations for twinning activation during uniaxial tensile or compression tests in L-PBF 316L. Indeed, mechanical twinning is an important deformation mechanism in L-PBF 316L steels, which also exhibit a strong crystallographic texture [10, 11]. To this purpose, SF_{RD} and SF_{ND} were computed on a standard triangle as shown in Figures 3a and 3b respectively.

Grains orientated with a $\langle 1\,1\,0 \rangle$ direction along the stress direction are favorable to mechanical twinning for a tensile test (Figure 3a), while grains orientated with a $\langle 1\,0\,0 \rangle$ direction along the stress direction are favorable for

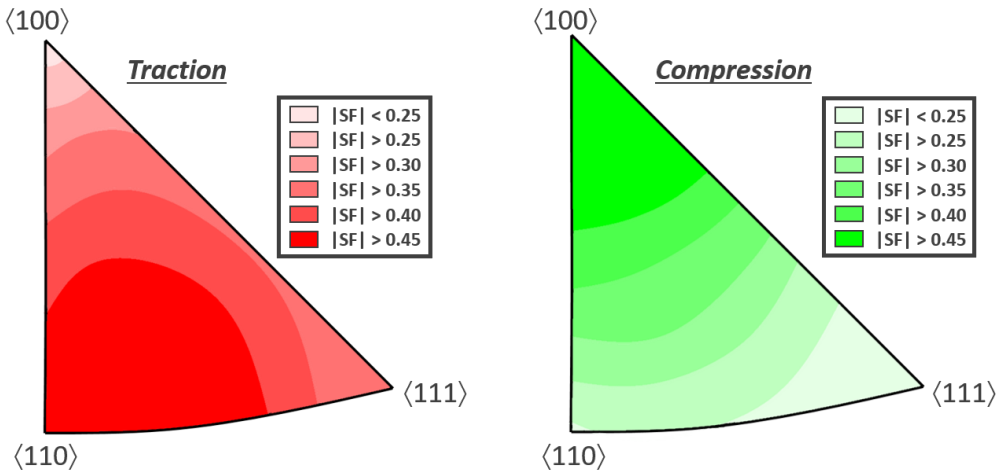

(a) (b)

Figure 3: Maximum SF values among the 12 twin variants as a function of the crystallographic orientation of the tensile direction (a) and compression direction (b).

mechanical twinning for a compression test (Figure 3b). Considering that 316L L-PBF steels can exhibit a strong $\langle 1\,1\,0 \rangle$ texture along the building direction [8, 12, 13], mechanical twinning can be more easily activated during tensile tests when the tensile direction is collinear to the building direction, thus leading to a better ductility. This phenomenon was especially observed by Wang et. al [11]: $\langle 1\,1\,0 \rangle$ specimens exhibited the highest ductility among other sample orientations such as $\langle 1\,0\,0 \rangle$ and $\langle 1\,1\,1 \rangle$. Moreover, $\langle 1\,0\,0 \rangle$ specimens have the lowest ductility, which can be explained by the very low SF_{RD} below 0.25, impeding twinning activation.

Furthermore, the competition between twinning and dislocation slip can be more easily analysed for uni-axial strains. For compressive state (Figure 3b), twinning is strongly favored for $\langle 1\,0\,0 \rangle$ direction and not favored for $\langle 1\,1\,0 \rangle$ direction, while SF values for dislocation slip are the same for these

two directions and near to the maximum (0.41) [14]. As we showed that the compressive component of rolling is the main contribution during rolling, the example of Figure 1 can be used to illustrate this point. On one hand, grains with $\langle 1\,1\,0 \rangle$ along ND (compression direction during rolling), such as grain C, do not exhibit twins due to a low SF value and are then only deformed by dislocation slip. On the other hand, grans with $\langle 1\,0\,0 \rangle$ along ND, such as grain A, are extensively twined while they should also experience dislocation slip. Hence, activation of twinning is then mainly due to crystallographic orientation and occurs independently to slip activity.

As a conclusion, the exposed method allows to reliably determine the activated twinning variant in cold-rolled fcc structures. This robust method can also be used in this regard for tensile or compressive uniaxial deformations. The modified effective Schmid factor is shown to be a relevant parameter to predict the activated twinning variant during cold-rolling. This study highlights that the compressive component is predominant in the cold-rolling deformation. The determination of the maximum Schmid factor values as a function of the orientation of the tensile and compression directions also outlines that mechanical twinning is favorable for a tensile direction along the $\langle 1\,1\,0 \rangle$ direction and a compressive direction along the $\langle 1\,0\,0 \rangle$ direction for a uniaxial deformation. In the specific case of L-PBF 316L steels with a strong $\langle 1\,1\,0 \rangle$ texture along the building direction, the highest ductility when tensile specimens are strained along this direction can be explained by intense twinning activation due to favorable grain orientations.

References

[1] G. Mani, M. D. Feldman, D. Patel, C. M. Agrawal, Coronary stents: A materials perspective, Biomaterials 28 (9) (2007) 1689–1710.

[2] T. Beck, V. Blanc, J.-M. Escleine, D. Haubensack, M. Pelletier, M. Phelip, B. Perrin, C. Venard, Conceptual design of ASTRID fuel subassemblies, Nucl. Eng. Des. 315 (2017) 51–60.

[3] X. Wu, X. Pan, J. C. Mabon, M. Li, J. F. Stubbins, The role of deformation mechanisms in flow localization of 316L stainless steel, J. Nucl. Mater. 356 (1-3) (2006) 70–77.

[4] M. Eskandari, A. Najafizadeh, A. Kermanpur, Effect of strain-induced martensite on the formation of nanocrystalline 316L stainless steel after cold rolling and annealing, Mater. Sci. Eng. A 519 (1-2) (2009) 46–50.

[5] E. Bertrand, P. Castany, I. Péron, T. Gloriant, Twinning system selection in a metastable β-titanium alloy by Schmid factor analysis, Scr. Mater. 64 (12) (2011) 1110–1113.

[6] T. Sawai, A. Hishinuma, Twin intersection in tensile deformed γ-tial intermetallic compounds, J. Phys. Chem. Solids 66 (2-4) (2005) 335–338.

[7] J. Luo, A. Godfrey, W. Liu, Q. Liu, Twinning behavior of a strongly basal textured AZ31 Mg alloy during warm rolling, Acta Mater. 60 (5) (2012) 1986–1998.

[8] L. Lemarquis, P. Giroux, H. Maskrot, B. Barkia, O. Hercher, P. Castany, Cold-rolling effects on the microstructure properties of 316L stainless steel parts produced by laser powder bed fusion (LPBF), J. Mater. Res. Technol. 15 (2021) 4725–4736.

[9] C. Zhang, D. Jensen, T. Yu, Effects of initial 3d printed microstructures on subsequent microstructural evolution in 316l stainless steel, Acta Mater. 242 (2023) 118481.

[10] M. Pham, B. Dovgyy, P. Hooper, Twinning induced plasticity in austenitic stainless steel 316L made by additive manufacturing, Mater. Sci. Eng. A 704 (2017) 102–111.

[11] X. Wang, J. A. Muniz-Lerma, M. A. Shandiz, O. Sanchez-Mata, M. Brochu, Crystallographic-orientation-dependent tensile behaviours of stainless steel 316L fabricated by laser powder bed fusion, Mater. Sci. Eng. A 766 (2019) 138395.

[12] J. J. Marattukalam, D. Karlsson, V. Pacheco, P. Beran, U. Wiklund, U. Jansson, B. Hjörvarsson, M. Sahlberg, The effect of laser scanning strategies on texture, mechanical properties, and site-specific grain orientation in selective laser melted 316L SS, Mater. Des. 193 (2020) 108852.

[13] S. Sun, T. Ishimoto, K. Hagihara, Y. Tsutsumi, T. Hanawa, T. Nakano, Excellent mechanical and corrosion properties of austenitic stainless steel with a unique crystallographic lamellar microstructure via selective laser melting, Scr. Mater. 159 (2019) 89–93.

[14] D. Barbier, N. Gey, N. Bozzolo, S. Allain, M. Humbert, EBSD for analysing the twinning microstructure in fine-grained twip steels and its influence on work hardening, J. Microsc. 235 (1) (2009) 67–78.